Nanoscale

PAPER

View Article Online
View Journal | View Issue

Cite this: *Nanoscale*, 2017, **9**, 4265

An origin of unintentional doping in transition metal dichalcogenides: the role of hydrogen impurities†

Youngho Kang and Seungwu Han*

Received 2nd November 2016,
Accepted 28th February 2017

DOI: 10.1039/c6nr08555e

rsc.li/nanoscale

We theoretically elucidate the origin of unintentional doping in two-dimensional transition-metal dichalcogenides (TMDs), which has been consistently reported by experiment, but which still remains unclear. Our explanation is based on the charge transfer between TMDs and the underlying SiO_2 in which hydrogen impurities with a negative-U property pin the Fermi level of the SiO_2 as well as adjacent TMD layers. Using first-principles calculations, we obtain the pinning point of the Fermi level from the charge transition level of the hydrogen in the SiO_2, $\varepsilon(+/-)$, and align it with respect to the band-edge positions of monolayer TMDs. The computational results show that the Fermi levels of TMDs estimated by $\varepsilon(+/-)$ successfully explain the conducting polarity (n- or p-type) and relative doping concentrations of thin TMD films. By enlightening on the microscopic origin of unintentional doping in TMDs, we believe that the present work will contribute to precise control of TMD-based electronic devices.

Introduction

Recently two-dimensional systems based on transition metal dichalcogenides (TMDs) have attracted a great deal of attention in nanoelectronics owing to their unique mechanical and electrical properties.[1–6] Structurally, two-dimensional layers in crystalline TMDs are bound by the weak van der Waals force, which facilitates exfoliation into a few layers or even a monolayer through various experimental techniques.[7,8] This also enables facile integration of TMDs into nanodevices with pre-designed heterostructures.[9–11] In addition, in contrast to the pristine graphene that is semi-metallic,[12] TMDs are intrinsic semiconductors with moderate band gaps over 1 eV.[13] Thus, they are expected to be well-suited for a two-dimensional channel layer in ultrathin body field-effect transistors (FETs) that can suppress short-channel effects at its scaling limits.[4,14,15]

Even though the potential of TMDs as two dimensional semiconductors was fully demonstrated by previous experiments, the understanding of their electronic properties is still insufficient. For example, numerous experimental studies on atomically thin TMD layers consistently observed n- or p-type behaviours without any intentional dopants,[1,5,16–21] but the doping mechanism of TMDs, which should be clarified for the precise control of TMD devices, remains unexplained.[5,19] According to experiments, conducting polarities (n- or p-type) and carrier concentrations of TMD films depend on the chemical composition of TMDs.[5] For example, current–voltage characteristics shift from n- to p-type as the material changes from MoS_2 (n-type) to $MoSe_2$ (bipolar) and $MoTe_2$ (p-type). In addition, it was shown that both MoS_2 and WS_2 exhibit n-type conductivity, but the carrier density is much larger in MoS_2.[17]

In order to reveal the microscopic origin of unintentional doping in TMD films, several defect structures were examined in previous density-functional theory (DFT) calculations: Noh *et al.* found that native defects such as Mo interstitial and S vacancy cannot account for the n-type property in MoS_2 since they produce midgap states in the band gap.[22] The influence of interstitial hydrogen was also examined as it is a well-known shallow donor in several n-type oxide semiconductors,[23,24] but it also turned out to be a deep donor.[25] As an extrinsic origin, Dolui *et al.* paid attention to the charge transfer between MoS_2 and oxide substrates because TMD films are usually supported by insulators such as SiO_2.[26] They explored possible defects at the SiO_2–MoS_2 interface and proposed that the Na contamination and oxygen dangling bonds at the surface of SiO_2 can cause n-type and p-type doping in MoS_2, respectively. However, the model cannot address the change of electrical polarity depending on the TMD species mentioned above.

Here, we theoretically propose an origin of unintentional doping in two-dimensional TMDs using DFT calculations,

Department of Materials Science and Engineering and Research Institute of Advanced Materials, Seoul National University, Seoul 151-744, Korea.
E-mail: hansw@snu.ac.kr

†Electronic supplementary information (ESI) available: Details of the computations and atomic structures, binding energy of SiO_2 and MoS_2, density of states of SiO_2 supercells with a hydrogen impurity, Poisson's equation solver. See DOI: 10.1039/c6nr08555e

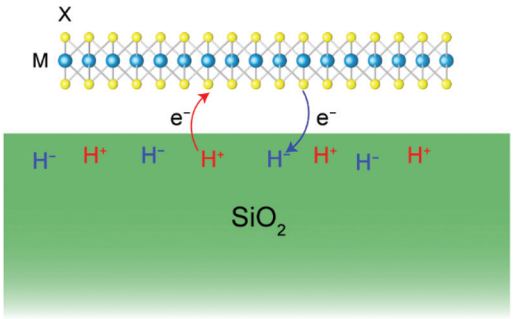

Fig. 1 Schematic for the charge transfer process between a TMD layer and hydrogen impurity in a SiO_2 substrate. M and X are metal and chalcogenide components in TMDs, respectively.

which can explain experimental observations consistently. We were motivated by a recent experiment showing that the SiO_2 substrate significantly affects doping in thin MoS_2 films by enhancing n-type conductivity.[19] At the heart of the present model is the notion that hydrogen impurities in the SiO_2 substrate are the source of electron or hole carriers in adjacent TMD layers because they cause the Fermi level (E_F) to be pinned at the interface. Fig. 1 illustrates this schematically. It is known that hydrogen can be easily introduced into SiO_2 during thermal oxidation with concentrations as high as 10^{18}–10^{21} cm^{-3}.[27–29] (H-contamination would be negligible during the deposition of TMDs on SiO_2 since sources containing hydrogen are usually avoided in CVD fabrication to exclude the formation of H_2S.[30]) We find that the electronic transition level of hydrogen impurities relative to band edges of TMDs successfully explains the doping type of TMDs observed in experiments, particularly the change of electrical polarity and carrier concentrations depending on the chemical composition of TMDs.

Results and discussion

All the calculations in this study are performed using a Vienna *ab initio* simulation package (VASP).[31] The projector-augmented-wave (PAW) pseudopotential is used for ionic potentials,[32] and 500 eV of cutoff energy is employed for the plane wave basis set. The PBE functional[33] is adopted for geometry optimization. Since PBE underestimates the band gap significantly, the final electronic structures and total energies are obtained by applying the HSE06 hybrid functional.[34] The results from this approach (the HSE calculations on geometries relaxed with PBE) are consistent with previous studies as discussed below, implying that further relaxation within HSE06 is not significant.

The fraction of Fock exchange in the hybrid functional calculation is often chosen to reproduce the experimental band gap, but we use the standard value of 25% throughout this work because there is no reliable experimental band gap (not optical gaps) of ultrathin TMDs in experiments due to difficulties in measurement.[35] The band gap of MoS_2 in the present HSE calculation is 2.14 eV (without spin–orbit coupling), which falls well into the range of corresponding GW band gaps considering substrate screening.[35–37] We also tested 30% of Fock exchange for MoS_2 but the main conclusion did not change. On the other hand, 25% mixing is insufficient to describe the experimental band gap of SiO_2 (9.3 eV),[38,39] but this is not crucial for the main conclusion, which will be discussed below.

The *k*-points are sampled to ensure the total energy convergence within 10 meV per atom. The spin–orbit interaction is taken into account in computing electronic band structures because it substantially affects the band edges of TMDs.[13,40] Experimentally, SiO_2 substrates are amorphous, but we adopt a crystalline SiO_2 with the α-quartz structure for computational convenience. In spite of differences in the long-range order, the electrical properties of hydrogen impurities in α-quartz are close to those in the amorphous phase.[41] The monolayer TMDs are modeled as the 1H phase for MoS_2, $MoSe_2$, $MoTe_2$, WS_2, WSe_2, WTe_2,[13] and SnS_2,[42] and as the 1T phase for ReS_2 [43] (see section 1 in the ESI† for more details about computations and atomic geometries).

Hydrogen in SiO_2 is amphoteric; it can act as both a donor (H^+) or an acceptor (H^-).[41,44] The preferential atomic site of hydrogen depends on its charge state such that H^+ and H^- form a chemical bond with oxygen and silicon, respectively, as shown in Fig. 2(a) and (b). The formation energy (E^f) that determines the thermodynamically stable charge state of hydrogen, is calculated by:[44]

$$E^f(H^q) = E_{tot}(H^q) - E_{tot}(\text{clean}) - \mu_H + qE_F, \quad (1)$$

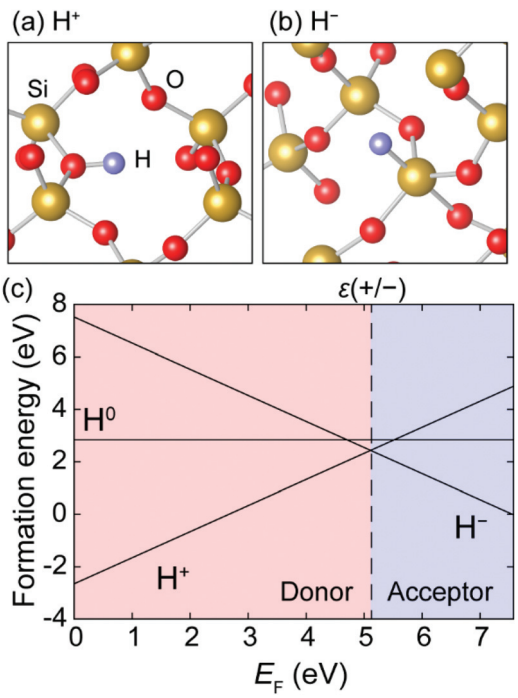

Fig. 2 Atomic configurations of hydrogen impurities in SiO_2 with (a) positive and (b) negative charge states. (c) Defect formation energy of hydrogen impurities in SiO_2 as a function of the Fermi level.

where q is the charge state, $E_{tot}(H^q)$ and E_{tot}(clean) are the total energy of supercells containing H^q and hydrogen-free SiO_2, respectively. In eqn (1), μ_H is the chemical potential of hydrogen and we fix it at half of the total energy of a H_2 molecule. We define E_F with respect to the valence band maximum (VBM) of SiO_2. The spurious electrostatic interaction between periodic images of charged defects is fixed by the Madelung correction scheme (see section 2 in the ESI† for details about the computation and resulting electronic structures of SiO_2 with a hydrogen impurity).[45]

Fig. 2(c) shows the E^f's of H^+ and H^- as a function of E_F. It is seen that hydrogen behaves as a donor when E_F is close to the valence band. However, when E_F increases across the band gap, the E^f of H^+ (H^-) increases (decreases). As a result, H^- is more favored than H^+ after E_F crosses the electronic transition level, $\varepsilon(+/-)$, that is given by

$$\varepsilon(+/-) = \{E_{tot}(H^-) - E_{tot}(H^+)\}/2 - \text{VBM}. \quad (2)$$

That is to say, the hydrogen in SiO_2 can trap electrons for $E_F > \varepsilon(+/-)$ and holes for $E_F < \varepsilon(+/-)$. The neutral state of hydrogen, H^0, is always higher in energy than H^+ or H^-, and this is called a negative-U behavior.[44] The negative-U property of hydrogen impurities implies that the E_F in SiO_2 is pinned to $\varepsilon(+/-)$ with a pinning strength depending on hydrogen concentrations.[44] Godet *et al.*[41] also reported the negative-U property of hydrogen in SiO_2, but the $\varepsilon(+/-)$ with respect to VBM was lower than our value because they used the GGA method which results in a smaller band gap of SiO_2 than the present one.

Hydrogen in SiO_2 can lead to doping of adjacent two-dimensional TMD layers by adjusting their Fermi levels to $\varepsilon(+/-)$ through charge transfer at the interface. This means that the energy alignment between the $\varepsilon(+/-)$ of SiO_2 and the band edges of TMDs will determine doping types of thin TMD layers. Although the interaction between MoS_2 and SiO_2 is of the van der Waals type that does not involve direct chemical bonds, 3 Å separation should allow charge transfer across the interface *via* the hopping process. We note that previous experiments have reported the charge transfer between van der Waals complexes and its influence on the properties of materials and related devices.[46–48] In particular, it is well known that the charge transfer between van der Waals complexes plays a key role in the carrier transport in organic semiconductors where the constituent molecules are bound to each other *via* the van der Waals force; a carrier can move molecule-to-molecule through the hopping process leading to an electric current when the electric field is applied.[49]

In the DFT calculation, the band alignment between two materials can be obtained *via* (1) making an interface model or (2) the vacuum level alignment from separate surface calculations. The former produces energy level alignment including interface effects such as interface dipoles that arise from redistribution of the charge density. On the other hand, the latter has advantages of computational simplicity. These two methods will produce identical energy alignments if the interface effects are negligible.

In order to examine the impacts of the interface on the level alignments between SiO_2 and TMDs, we first model the interface for SiO_2/MoS_2 where the oxygen-terminated SiO_2(0001) surface with silanol groups (Si–OH) {see Fig. 3(a)} interacts with monolayer MoS_2 {see section 3 in the ESI† for details about the computations of the SiO_2(0001) surface}. Since the theoretical lattice parameters of MoS_2 and SiO_2 are 3.18 and 5.01 Å, respectively, the supercell is constructed by combining the 3 × 3 cells of the MoS_2 monolayer and 2 × 2 cells of the SiO_2(0001) surface. The in-plane lattice parameter of the supercell is set to that of the MoS_2 but the results are the same if it is adjusted to that of SiO_2. The equilibrium distance between the SiO_2 and the MoS_2 is calculated by including van der Waals forces based on the non-local van der Waals density functional (vdW-DF).[50] The equilibrium distance from the topmost O atom to the closest S layer of MoS_2 is 3.0 Å with a small binding energy of 16 meV $Å^{-2}$, confirming that MoS_2 is weakly bound to the underlying SiO_2 by the van der Waals forces (see section 4 in the ESI† for more details about the interface calculation).

We compare the band alignment in the interface model with that obtained by aligning the vacuum level in separate surface calculations, and it is found that they agree well within 0.1 eV. This is in line with a recent experimental result showing that the interaction between SiO_2 and MoS_2 is negligible.[51] Thus, in the following, we align the $\varepsilon(+/-)$ of SiO_2 and the band edges of TMDs from the separate surface models of SiO_2 and TMDs, rather than constructing the actual interface models.

For the surface model of SiO_2, we adopt the oxygen-terminated SiO_2(0001) 2 × 2 surface with siloxane groups (Si–O–Si) forming six-membered ring structures[26,52] as shown in Fig. 3(b) in addition to the 1 × 1 surface with silanol groups

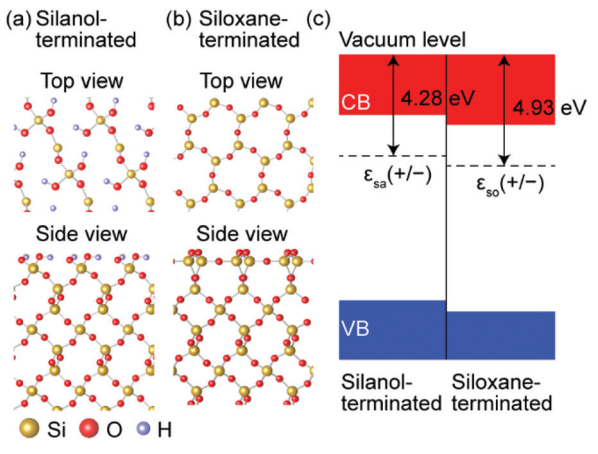

Fig. 3 Top and side views of O-terminated SiO_2(0001) surfaces with (a) silanol and (b) siloxane. For the siloxane group, the surface is reconstructed into six-membered ring structures. (c) The charge transition levels of hydrogen referenced to the vacuum level of silanol, $\varepsilon_{sa}(+/-)$, and siloxane, $\varepsilon_{so}(+/-)$, surfaces.

employed in the above. Since our models contain symmetric surfaces, the dipole correction is not necessary. Both surfaces were observed in experiments depending on their surface treatments.[53–55] Fig. 3(c) shows $\varepsilon(+/-)$ with respect to the vacuum level for each surface. It is found that the surface with siloxane groups results in a lower electronic transition level, $\varepsilon_{so}(+/-)$ than that of the surface with silanol groups, $\varepsilon_{sa}(+/-)$. This is because the surface dipole in the siloxane surface points into SiO_2, which shifts up the vacuum level compared with the silanol surface.

As we mentioned earlier, the band gap of SiO_2 in the present HSE calculation underestimates the experimental value. However, we note that $\varepsilon_{so}(+/-)$ and $\varepsilon_{sa}(+/-)$ are weakly dependent upon the exchange–correlation functional if they are referenced to the vacuum level. For instance, the $\varepsilon_{sa}(+/-)$ and $\varepsilon_{so}(+/-)$ in the PBE calculations differ from the HSE results in Fig. 3(c) by only 0.06 eV. This is because both functionals identically describe the energy difference between the distinct charge states of a localized defect.[56] Therefore, our conclusion is not sensitive to the fraction of Fock exchange.

Fig. 4(a) shows the electronic transition levels of hydrogen for each surface termination and band offsets of various TMDs with respect to the vacuum level. Since the siloxane and silanol groups usually coexist in the amorphous SiO_2 in experiments,[54] the transition level in real systems may lie somewhere between $\varepsilon_{so}(+/-)$ and $\varepsilon_{sa}(+/-)$ and locally fluctuate due to the non-uniformity of surface structures. As such, we also mark the average value of $\varepsilon_{so}(+/-)$ and $\varepsilon_{sa}(+/-)$ as $\varepsilon_{ave}(+/-)$ that may correspond to the averaged Fermi level of TMDs. To show the doping polarity more clearly, we define the relative Fermi level (E_F^{rel}) as $E_F^{rel} = [\varepsilon_{ave}(+/-) - \{E_g/2 + VBM\}]/E_g$, where E_g are the band gaps of TMD, respectively {see Fig. 4(b)}. It is noted that E_F^{rel} becomes 0.5 (−0.5) when $\varepsilon_{ave}(+/-)$ lies at the bottom of the conduction band (top of the valence band) of TMDs.

To check whether the separate surface calculations employed in this work are still valid in the presence of hydrogen impurities, we perform a test, PBE calculation, on $\varepsilon_{sa}(+/-)$ using a full interface model of MoS_2/SiO_2 that explicitly includes a hydrogen atom in SiO_2 (see section 5 in the ESI† for details). It turns out that $\varepsilon_{sa}(+/-)$ lies at 0.03 eV above the conduction band minimum (CBM) of MoS_2, which agrees with the separate calculations using the same functional in which $\varepsilon_{sa}(+/-)$ is located at 0.05 eV higher than CBM of MoS_2. This implies that the decoupling approximation gives results that are equivalent to those of the full calculations.

So far, the theoretical model only concerned the monolayer TMDs. For multilayer TMDs, it is known that the band gap becomes smaller than for the monolayer because of diminishing quantum confinement effects.[13] In addition, the conduction and valence band edges shift in the opposite direction by similar amounts.[13] Therefore, multilayer TMDs are expected to exhibit the same polarity as monolayer structures, but show larger carrier concentrations. This is consistent with a recent experiment where MoS_2 exhibits a larger conductivity in multilayers than in the monolayers.[57]

Now we compare the main results in Fig. 4 with extant experimental observations. As mentioned earlier, previous experiments reported that the atomically thin MoS_2 layer placed on the SiO_2 substrate typically shows an n-type character and the Fermi level of the monolayer MoS_2 lies close to the CBM.[1,3,6,10,11,17,19] This is consistent with the present results because $\varepsilon_{ave}(+/-)$ is near the conduction band edge of the MoS_2. We also note that the band edges of the TMDs gradually upshift as the chalcogenide element goes down from S to Te. (This was also found in a previous HSE calculation.[13]) As a result, $\varepsilon_{ave}(+/-)$ lies near the conduction band in the MoS_2 while it is close to the valence band in the $MoTe_2$. This implies that the doping type changes from n- to p-type as can be seen in Fig. 4(b). This result well explains the evolution of conduction polarity in Mo-based TMD films in experiments.[5] Furthermore, $\varepsilon_{ave}(+/-)$ is found to be closer to the conduction band of MoS_2 than that of WS_2. This is also consistent with the experimental finding that the carrier density of WS_2 is lower than that of MoS_2 while both TMDs exhibit an n-type behavior on SiO_2.[17] In Fig. 4(b), $\varepsilon_{ave}(+/-)$ lies close to the valence band of the WSe_2, indicating a p-type WSe_2 on the SiO_2 sub-

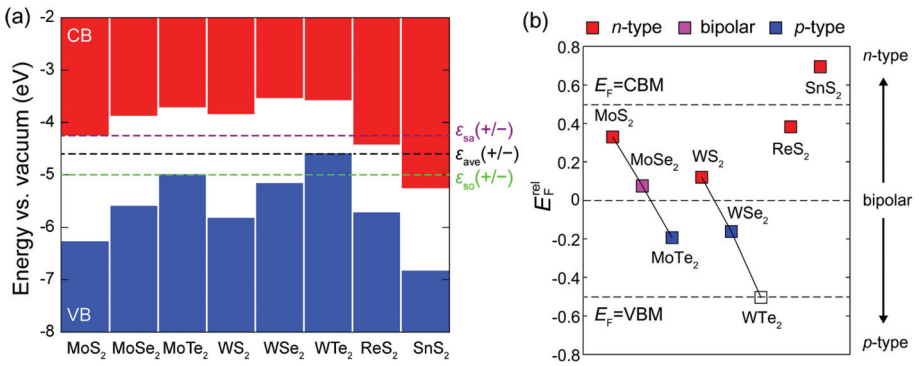

Fig. 4 (a) Energy level alignment between the electronic transition level of hydrogen and band edges of monolayer TMDs. $\varepsilon_{ave}(+/-)$ corresponds to the average of $\varepsilon_{sa}(+/-)$ and $\varepsilon_{so}(+/-)$. (b) The relative Fermi level (E_F^{rel}) of TMDs. This becomes positive (negative) if system is n (p)-type doped. The color in square denotes the electrical polarity observed in experiments (we are missing the color for WTe_2 because its electrical polarity has not been reported yet).[1,3,5,6,10,11,16,17,19,20,42,60]

strate, in agreement with experiments.[16] However, one may expect bipolar characteristics for WS_2 and WSe_2 because their E_F^{rel}'s are not significantly different from that of $MoSe_2$. Indeed, one recent experiment reported that WS_2 showed mainly an n-type behavior, but a weak bipolar behavior as well.[58]

To the best of our knowledge, the electrical polarity of WTe_2 with the 1H phase has not been measured yet even though this phase was identified experimentally. This is attributed to the fact that WTe_2 is the most stable in a distorted 1T phase, showing a semimetallic property.[59] We expect that the 1H-WTe_2 on the SiO_2 substrate will exhibit p-type conductivity more strongly than $MoTe_2$ and WSe_2.

To further validate the present model, we also examine the doping behavior of ReS_2 and SnS_2 that do not include Mo and W. As shown in Fig. 4(a), both ReS_2 and SnS_2 display n-type property when they are placed on the SiO_2 substrate because $\varepsilon_{ave}(+/-)$ is near (ReS_2) or even above (SnS_2) the conduction band minimum. Indeed, recent experiments demonstrated that thin ReS_2 and SnS_2 films show n-type conductivity.[42,60]

The conductivity of TMDs typically increases with temperature,[61,62] which can be attributed to the multiplication of carrier densities through thermal activation. In addition to this, there is an intriguing temperature effect: according to Jiang *et al.*,[61] the MoS_2 thin-film transistor displayed a memory step above 450 K, in which the current level at zero gate voltage is abruptly enhanced in comparison with those at lower temperatures during the gate-voltage sweep. We conjecture that the hydrogen in SiO_2 could be involved in this phenomenon because hydrogen is known to be mobile in oxides above room temperature[63] as well as enable control of the conductivity of TMDs *via* trapping carriers or modulating interface dipoles.

One may raise a question regarding the amount of hydrogen density necessary to dope TMDs. To this end, we evaluated the Fermi level of MoS_2 using a home-made solver of the Poisson's equation for a MoS_2–SiO_2 interface model (see section 6 in the ESI† for more details). This solver calculates the Fermi level of MoS_2 in a self-consistent way by considering the charge transfer, and resulting interface dipole and band bending. These results show that the Fermi level of MoS_2 appears near the conduction band minimum as shown in Fig. 4(a) even for very small hydrogen concentrations of 10^{10}–10^{12} cm^{-3}. Such a facile pinning is a result of the two-dimensional nature of TMDs.

Finally, we point out that the energetic position of $\varepsilon_{ave}(+/-)$, a key quantity to explain the doping properties of adjacent TMD layers, is about 4.6 eV below the vacuum level. Interestingly, this value is close to the standard water redox potential, 4.44 eV. This is not a coincidence, as mentioned in ref. 44, that demonstrated universality in $\varepsilon(+/-)$ of hydrogen over a wide range of materials including water.[44] The absolute transition level may vary depending on the surface dipole, but on average, it would not significantly deviate from 4.44 eV below the vacuum level. This also implies that other oxide substrates can lead to similar doping behaviors as SiO_2. In this respect, it can be understood why thin MoS_2 films in contact with high-k dielectric oxides such as Al_2O_3 [10,64] and HfO_2 [1,3] are also found to be n-type.

Conclusions

In summary, we theoretically investigated the origin of unintentional doping of atomically thin TMDs. We proposed that the charge transfer occurs at the SiO_2/TMD interface because of the amphoteric nature of hydrogen impurities in SiO_2. This means that the doping polarity depends on the relative position of the $\varepsilon(+/-)$ of hydrogen within the band gap of TMDs. By aligning the $\varepsilon(+/-)$ and band edges of TMDs through surface models, we were able to explain every unintentional doping of TMDs observed in experiments. This strongly implies that the hydrogen in underlying substrates is responsible for the unintentional doping in TMD films. Our results indicate that the electrical properties of TMDs can be tuned by changing the vacuum level of substrates, *i.e.*, the position of the $\varepsilon(+/-)$ of the hydrogen in substrates relative to the band edges of TMDs. This implies the possibility of a new doping strategy for atomically thin TMD films. For example, the hole (electron) concentration of TMDs could be enlarged (reduced) if the surface of substrates is decorated by strongly electronegative anions like halogens that usually increase the work function by shifting the vacuum level upward.[65]

Acknowledgements

This work was supported by the Samsung Research Funding Center of Samsung Electronics. The computations were performed at the KISTI supercomputing center (Grant No. KSC-2015-C3-038).

Notes and references

1 B. Radisavljevic, A. Radenovic, J. Brivio, V. Giacometti and A. Kis, *Nat. Nanotechnol.*, 2011, **6**, 147.
2 G. Fiori, F. Bonaccorso, G. Iannaccone, T. Palacios, D. Neumaier, A. Seabaugh, S. K. Banerjee and L. Colombo, *Nat. Nanotechnol.*, 2014, **9**, 768.
3 Y. Yoon, K. Ganapathi and S. Salahuddin, *Nano Lett.*, 2011, **11**, 3768.
4 H. Wang, L. Yu, Y.-H. Lee, Y. Shi, A. Hsu, M. L. Chin, L.-J. Li, M. Dubey, J. Kong and T. Palacios, *Nano Lett.*, 2012, **12**, 4674.
5 N. R. Pradhan, D. Rhodes, Y. Xin, S. Memaran, L. Bhaskaran, M. Siddiq, S. Hill, P. M. Ajayan and L. Balicas, *ACS Nano*, 2014, **8**, 7923.
6 H. Liu, A. T. Neal and P. D. Ye, *ACS Nano*, 2012, **6**, 8563.
7 K. S. Novoselov, D. Jiang, F. Schedin, T. J. Booth, V. V. Khotkevich, S. V. Morozov and A. K. Geim, *Proc. Natl. Acad. Sci. U. S. A.*, 2005, **102**, 10451.

8 P. Joensen, R. F. Frindt and S. R. Morrison, *Mater. Res. Bull.*, 1986, **21**, 457.
9 L. Britnell, R. M. Ribeiro, A. Eckmann, R. Jalil, B. D. Belle, A. Mishchenko, Y.-J. Kim, R. V. Gorbachev, T. Georgiou, S. V. Morozov, A. N. Grigorenko, A. K. Geim, C. Casiraghi, A. H. Castro Neto and K. S. Novoselov, *Science*, 2013, **340**, 1311.
10 S. Das, H.-Y. Chen, A. V. Penumatcha and J. Appenzeller, *Nano Lett.*, 2013, **13**, 100.
11 Z. Yin, H. Li, H. Li, L. Jiang, Y. Shi, Y. Sun, G. Lu, Q. Zhang, X. Chen and H. Zhang, *ACS Nano*, 2012, **6**, 74.
12 F. Schwierz, *Nat. Nanotechnol.*, 2010, **5**, 487.
13 J. Kang, S. Tongay, J. Zhou, J. Li and J. Wu, *Appl. Phys. Lett.*, 2013, **102**, 012111.
14 F. Schwierz, J. Pezoldt and R. Granzner, *Nanoscale*, 2015, **7**, 8261.
15 X. Duan, C. Wang, A. Pan, R. Yu and X. Duan, *Chem. Soc. Rev.*, 2015, **44**, 8859.
16 N. R. Pradhan, D. Rhodes, S. Memaran, J. M. Poumirol, D. Smirnov, S. Talapatra, S. Feng, N. Perea-Lopez, A. L. Elias, M. Terrones, P. M. Ajayan and L. Balicas, *Sci. Rep.*, 2015, **5**, 8979.
17 L. Yang, K. Majumdar, H. Liu, Y. Du, H. Wu, M. Hatzistergos, P. Y. Hung, R. Tieckelmann, W. Tsai, C. Hobbs and P. D. Ye, *Nano Lett.*, 2014, **14**, 6275.
18 X. Lu, M. I. B. Utama, J. Lin, X. Gong, J. Zhang, Y. Zhao, S. T. Pantelides, J. Wang, Z. Dong, Z. Liu, W. Zhou and Q. Xiong, *Nano Lett.*, 2014, **14**, 2419.
19 C.-P. Lu, G. Li, J. Mao, L.-M. Wang and E. Y. Andrei, *Nano Lett.*, 2014, **14**, 4628.
20 L. Zhou, K. Xu, A. Zubair, A. D. Liao, W. Fang, F. Ouyang, Y.-H. Lee, K. Ueno, R. Saito, T. Palacios, J. Kong and M. S. Dresselhaus, *J. Am. Chem. Soc.*, 2015, **137**, 11892.
21 D. Ovchinnikov, A. Allain, Y.-S. Huang, D. Dumcenco and A. Kis, *ACS Nano*, 2014, **8**, 8174.
22 J. Y. Noh, H. Kim and Y. S. Kim, *Phys. Rev. B: Condens. Matter*, 2014, **89**, 205417.
23 Y. Kang, B. D. Ahn, J. H. Song, Y. G. Mo, H.-H. Nahm, S. Han and J. K. Jeong, *Adv. Electron. Mater.*, 2015, **1**, 1400006.
24 C. G. Van de Walle, *Phys. Rev. Lett.*, 2000, **85**, 1012.
25 K. Dolui, I. Rungger, C. Das Pemmaraju and S. Sanvito, *Phys. Rev. B: Condens. Matter*, 2013, **88**, 075420.
26 K. Dolui, I. Rungger and S. Sanvito, *Phys. Rev. B: Condens. Matter*, 2013, **87**, 165402.
27 A. Yokozawa and Y. Miyamoto, *Phys. Rev. B: Condens. Matter*, 1997, **55**, 13783.
28 A. G. Revesz, *J. Electrochem. Soc.*, 1979, **126**, 122.
29 Y. Nagasawa, I. Yoshii, K. Naruke, K. Yamamoto, H. Ishida and A. Ishitani, *J. Appl. Phys.*, 1990, **68**, 1429.
30 B. H. Kim, M. Park, M. Lee, S. J. Baek, H. Y. Jeong, M. Choi, S. J. Chang, W. G. Hong, T. K. Kim, H. R. Moon, Y. W. Park, N. Park and Y. Jun, *RSC Adv.*, 2013, **3**, 18424.
31 G. Kresse and J. Furthmüller, *Phys. Rev. B: Condens. Matter*, 1996, **54**, 11169.
32 G. Kresse and D. Joubert, *Phys. Rev. B: Condens. Matter*, 1999, **59**, 1758.
33 J. P. Perdew, K. Burke and M. Ernzerhof, *Phys. Rev. Lett.*, 1996, **77**, 3865.
34 J. Heyd, G. E. Scuseria and M. Ernzerhof, *J. Chem. Phys.*, 2006, **124**, 219906.
35 D. Y. Qui, F. H. da Jornada and S. G. Louie, *Phys. Rev. B: Condens. Matter*, 2016, **93**, 235435.
36 F. Hüser, T. Olsen and K. S. Thygesen, *Phys. Rev. B: Condens. Matter*, 2013, **88**, 245309.
37 J. Ryou, Y.-S. Kim, S. KC and K. Cho, *Sci. Rep.*, 2016, **6**, 29184.
38 Z. A. Weinberg, G. W. Rubloff and E. Bassous, *Phys. Rev. B: Condens. Matter*, 1979, **19**, 3107.
39 S. Park, B. Lee, S. H. Jeon and S. Han, *Curr. Appl. Phys.*, 2011, **11**, S337.
40 S. Tongay, J. Zhou, C. Ataca, K. Lo, T. S. Matthews, J. Li, J. C. Grossman and J. Wu, *Nano Lett.*, 2012, **12**, 5576.
41 J. Godet and A. Pasquarello, *Microelectron Eng.*, 2005, **80**, 288.
42 Y. Huang, E. Sutter, J. T. Sadowski, M. Cotlet, O. L. A. Monti, D. A. Racke, M. R. Neupane, D. Wickramaratne, R. K. Lake, B. A. Parkinson and P. Sutter, *ACS Nano*, 2014, **8**, 10743.
43 S. Tongay, H. Sahin, C. Ko, A. Luce, W. Fan, K. Liu, J. Zhou, Y.-S. Huang, C.-H. Ho, J. Yan, D. F. Ogletree, S. Aloni, J. Ji, S. Li, J. Li, F. M. Peeters and J. Wu, *Nat. Commun.*, 2014, **5**, 3252.
44 C. G. Van de Walle and J. Neugebauer, *Nature*, 2003, **423**, 626.
45 G. Makov and M. C. Payne, *Phys. Rev. B: Condens. Matter*, 1995, **51**, 4014.
46 J. He, N. Kumar, M. Z. Bellus, H.-Y. Chiu, D. He, Y. Wang and H. Zhao, *Nat. Commun.*, 2014, **5**, 5622.
47 M. M. Furchi, A. Pospischil, F. Libisch, J. Burgdörfer and T. Mueller, *Nano Lett.*, 2014, **14**, 4785.
48 M. Muruganathan, J. Sun, T. Imamura and H. Mizuta, *Nano Lett.*, 2015, **15**, 8176.
49 P. Friederich, F. Symalla, V. Meded, T. Neumann and W. Wenzel, *J. Comp. Theory, Comput.*, 2014, **10**, 3720.
50 J. Klimeš, D. R. Bowler and A. Michaelides, *J. Phys.: Condens. Matter*, 2010, **22**, 022201.
51 S. W. Han, H. Kwon, S. K. Kim, S. Ryu, W. S. Yun, D. H. Kim, J. H. Hwang, J.-S. Kang, J. Baik, H. J. Shin and S. C. Hong, *Phys. Rev. B: Condens. Matter*, 2011, **84**, 045409.
52 T. C. Nguyen, M. Otani and S. Okada, *Phys. Rev. Lett.*, 2011, **106**, 106801.
53 K. Nagashio, T. Yamashita, T. Nishimura, K. Kita and A. Toriumi, *J. Appl. Phys.*, 2011, **110**, 024513.
54 A. S. D'Souza and C. G. Pantano, *J. Am. Ceram. Soc.*, 1999, **82**, 1289.
55 R. K. Iler, *The Chemistry of Silica*, Wiley-Interscience, New York, 1979.
56 A. Alkauskas and A. Pasquarello, *Phys. Rev. B: Condens. Matter*, 2011, **84**, 125206.
57 M.-W. Lin, I. I. Kravchenko, J. Fowlkes, X. Li, A. A. Puretzky, C. M. Rouleau, D. B. Geohegan and K. Xiao, *Nanotechnology*, 2016, **27**, 165203.

58 X. Liu, J. Hu, C. Yue, N. D. Fera, Y. Ling, Z. Mao and J. Wei, *ACS Nano*, 2014, **8**, 10396.
59 C.-H. Lee, E. C. Silva, L. Calderin, M. A. T. Nguyen, M. J. Hollander, B. Bersch, T. E. Mallouk and J. A. Robinson, *Sci. Rep.*, 2015, **5**, 10013.
60 C. M. Corbett, C. McClellan, A. Rai, S. S. Sonde, E. Tutuc and S. K. Banerjee, *ACS Nano*, 2015, **9**, 363.
61 C. Jiang, S. L. Rumyantsev, R. Samnakay, M. S. Shur and A. A. Balandin, *J. Appl. Phys.*, 2015, **117**, 064301.
62 D. Ovchinnikov, A. Allain, Y.-S. Huang, D. Dumcenco and A. Kis, *ACS Nano*, 2014, **8**, 8174.
63 J. B. Varley, H. Peelaers, A. Janotti and C. G. Van de Walle, *J. Phys.: Condens. Matter*, 2011, **23**, 334212.
64 S. Kim, A. Konar, W.-S. Hwang, J. H. Lee, J. Lee, J. Yang, C. Jung, H. Kim, J.-B. Yoo, J.-Y. Choi, Y. W. Jin, S. Y. Lee, D. Jena, W. Choi and K. Kim, *Nat. Commun.*, 2012, **3**, 1011.
65 M. G. Helander, Z. B. Wang, J. Qiu, M. T. Greiner, D. P. Puzzo, Z. W. Liu and Z. H. Lu, *Science*, 2011, **332**, 944.